CHIN. PHYS. LETT. Vol. 38, No. 4 (2021) 046201

Superior Mechanical Properties of GaAs Driven by Lattice Nanotwinning

Zhenjiang Han(韩振江)[1], Han Liu(刘晗)[1], Quan Li(李全)[1], Dan Zhou(周丹)[1,2*], and Jian Lv(吕健)[1*]

[1]*International Center for Computational Physics Method and Software, State Key Laboratory of Superhard Materials, Key Laboratory of Automobile Materials of MOE, and Department of Materials Science, Jilin University, Changchun 130012, China*

[2]*School of Science, Changchun University of Science and Technology, Changchun 130022, China*

(Received 11 January 2021; accepted 8 February 2021; published online 6 April 2021)

Gallium arsenide (GaAs), a typical covalent semiconductor, is widely used in the electronic industry, owing to its superior electron transport properties. However, its brittle nature is a drawback that has so far significantly limited its application. An exploration of the structural deformation modes of GaAs under large strain at the atomic level, and the formulation of strategies to enhance its mechanical properties is highly desirable. The stress-strain relations and deformation modes of single-crystal and nanotwinned GaAs under various loading conditions are systematically investigated, using first-principles calculations. Our results show that the ideal strengths of nanotwinned GaAs are 14% and 15% higher than that of single-crystal GaAs under pure and indentation shear strains, respectively, without producing a significantly negative effect in terms of its electronic performance. The enhancement in strength stems from the rearrangement of directional covalent bonds at the twin boundary. Our results offer a fundamental understanding of the mechanical properties of single crystal GaAs, and provide insights into the strengthening mechanism of nanotwinned GaAs, which could prove highly beneficial in terms of developing reliable electronic devices.

DOI: 10.1088/0256-307X/38/4/046201

Ⅲ–V binary semiconductors have attracted considerable attention on the basis of their potential industrial applications, such as light-emitting diodes, lasers and photo-detectors.[1−5] Gallium arsenide (GaAs) is one of the most promising candidates among Ⅲ–V direct-bandgap semiconductors, owing to its high carrier mobility and electron mobility,[6,7] superior to those of silicon, and as such, it has been widely used in many fields, including substrate materials,[8,9] solar cell fabrication,[10] and efficient photovoltaic devices.[11,12] Recently, a great deal of theoretical and experimental research has been devoted to detailed studies of the fundamental electronic properties and potential applications of GaAs in devices, including the effective modulation of band-gap engineering.[13−15] However, the drawback of its brittle nature, leading to a rapid deterioration in material performance, and accelerating the failure of devices, has significantly limited its potential application in industry.[16,17]

Grain boundaries play a pivotal role in strengthening metals or covalent solids;[18−21] this is achieved by suppressing the motion of dislocations. In recent years, experimental and theoretical studies have demonstrated that twin boundaries display much greater strength, as compared with grain boundaries in general.[22−26] For example, the tensile strength of nanotwinned Cu is ten times greater than that of ultrafine-grained Cu.[27] The twin boundary in diamond produces an unprecedented Vickers hardness (i.e., the quotient obtained by dividing the smoothly applied load by the square mm area of a pyramid-shaped diamond indenter), in excess of 200 GPa, significantly surpassing the hardness of all previously reported materials.[28] The Vickers hardness of nanotwinned cubic boron nitrides (BN) can be as much as 108 GPa, rivaling the hardness of natural diamond; this stems from the anisotropic shear stress response, which gradually turns weak bonding into hard bonding.[29] Theoretical simulations indicate that the strength of nanotwinned InSb is 11% higher than that of the flawless crystal.[30] BN and InSb are both Ⅲ–V compounds; however, their nanotwinned structures have a distinctive mechanism in terms of strength enhancement. Therefore, it is highly relevant to obtain a complete understanding for the mechanical properties of GaAs, which is located between BN and InSb in the periodic table, and to put forward a strategy to enhance its mechanical properties.

In this work, first-principles calculations are employed to examine the stress-strain relationships and failure mechanisms of flawless GaAs and nanotwinned

Supported by the National Key Research and Development Program of China (Grant No. 2018YFA0703400), the National Natural Science Foundation of China (Grant Nos. 11704044 and 11974134), the Jilin Province Outstanding Young Talents Project (Grant No. 20190103040JH), and the China Postdoctoral Science Foundation (Grant No. 2018M631870).

*Corresponding authors. Email: zhoudan@cust.edu.cn; lvjian@calypso.cn

© 2021 Chinese Physical Society and IOP Publishing Ltd

GaAs, under a variety of loading conditions. Our research reveals that the ideal pure shear strength of flawless GaAs is 5.15 GPa, whereas the pure shear strength of the nanotwinned GaAs structure is 5.87 GPa, 14% higher than that of the flawless crystal. The Vickers strength of nanotwinned GaAs is 15% higher than that of flawless GaAs. These strengthening mechanisms stem from directional covalent bond rearrangements at the twin boundaries, which may be applicable to the design and development of robust semiconductor devices.

Computational Methods. All calculations in this work were performed using the Vienna *ab initio* simulation package (VASP), based on density functional theory (DFT), in conjunction with the Perdew–Burke–Ernzerhof (PBE) generalized gradient approximation for electronic exchange and correlation interaction.[31–34] An energy cutoff of 600 eV, and Monkhorst–Pack (MP) k-point mesh, with a grid of 0.15 Å^{-1} and 0.2 Å^{-1}, for Brillouin zone (BZ) sampling were selected for both the flawless crystal and nanotwinned GaAs, respectively. The convergence for terminating the electronic self-consistent field and the force criterion on each atom were set to less than 1×10^{-5} eV and 1×10^{-2} eV/Å, respectively. To examine the mechanical response and failure mechanism of single crystalline and nanotwinned GaAs, stress-strain relations were calculated under various loading conditions, using a quasistatic relaxation method.[35–40] The deformed unit cell and atomic relaxation were examined at each step.[41] The pure shear deformation imposes shear strain on a particular slip system, while allowing the other five strain components to fully relax.[42,43] The biaxial shear (Vickers) deformation aims to mimic the stress conditions in Vickers indentation experiments, constraining the ratio of shear stress to normal stress and relating it to the geometry of the indenter, while the structure is relaxed along the four other strain components.[44–46] Vickers shear stress (Vickers stress) is the relaxed residual shear stress under biaxial deformation, and the Vickers strength of a material is the maximum Vickers stress for relaxation under biaxial deformation.

Results and Discussion. The single crystal of GaAs has a cubic structure, which is its thermodynamically stable phase under ambient conditions, and belongs to the space group $F\bar{4}3\,\text{m}$ (space group No. 216). The unit cell contains 4 Ga and 4 As atoms, with a 2.45 Å bond length in the Ga-As atoms. Our calculation produces an optimized lattice parameter of 5.75 Å, which is in excellent agreement with the experimental value of 5.65 Å,[47] verifying the reliability of our theoretical simulations. The calculated elastic constants of GaAs using the strain-stress method are listed as follows: $C_{11} = 99.61$ GPa, $C_{12} = 43.33$ GPa, and $C_{44} = 50.80$ GPa, satisfying the elastic stability criteria.[48] The theoretical bulk modulus B, shear modulus G, and Young's modulus E, derived from the Voigt–Reuss–Hill averaging scheme,[49] are 62.08, 40.08, and 98.95 GPa, in excellent agreement with the previous experimental results of 78.4, 47.1, and 117.7 GPa, respectively.[50] Using a well-developed semi-empirical hardness model,[51] the simulated Vickers hardness of single crystalline GaAs is 7.4 GPa, in good agreement with an experimental result of 7.5 GPa.[52]

To better understand the mechanical properties of GaAs under deformation, we systematically determine the stress–strain relations of single crystalline GaAs under tensile, pure shear, and (Vickers) indentation shear deformations along various slip systems.[53]

We first investigate the tensile stress-strain relations of GaAs along its high-symmetry orientations, including [001], [110], [111], and [11$\bar{2}$] so as to find the easy cleavage plane. The calculated results illustrate that the [111] direction has the lowest peak stress, being 11.01 GPa at a critical tensile strain of 0.15, as shown in Fig. 1, indicating that [111] is the weakest tensile direction; as such, the (111) plane is the most plausible slip plane for GaAs. This easy cleavage plane also exists in other covalent solids of similar compounds, e.g., BN and diamond.[29,54,55] The [001] direction has the highest tensile strength, being 16.45 GPa at a strain of 0.25, which is 49.4% larger than that for the [111] plane. This indicates significant anisotropy in terms of tensile strength. Moreover, the [111] and [11$\bar{2}$] directions exhibit similar peak stress under tensile strain. Note that all direction curves display an approximately linear stress response under small strain. To explore its atomic mechanisms, the structural evolution and bond length of flawless GaAs along the [111] direction are examined, as presented in the middle and right columns of Fig. 1, respectively. With increasing strain, the structure continuously resists deformation without bond breakage. The tension along [111] direction elongates the As1–Ga1 bond, with a concomitant shortening of the As1–Ga2 bond.

Next, we calculated the pure shear-stress-shear-strain curves of GaAs for various slip systems. Of all the pure shear calculated curves, the (111) $\langle 11\bar{2}\rangle$ shear direction exhibited the lowest peak stress, being 5.15 GPa at a pure shear strain of 0.32, suggesting that this direction is the most plausible slip system. The ideal pure shear stress of the (111) $\langle \bar{1}\bar{1}2\rangle$ slip system is 8.29 GPa at a strain of 0.29, which is 61.0% higher than the opposite to the directions of the (111) $\langle 11\bar{2}\rangle$ slip system, but significantly lower than that found for the (110) $\langle 001\rangle$, (11$\bar{2}$) $\langle \bar{1}\bar{1}\bar{1}\rangle$ and (001) $\langle 110\rangle$ systems. All stress increases with an increase in shear strain until the point of peak stress, indicating that the structure continuously resists deformation. Beyond the point of peak stress, the shear stress gradually decreases, suggesting structural soft-

ening. We also examined the structural evolution and bond changes under two shear deformations along the slip system with the weakest stress. The structure along the (111) $\langle 11\bar{2}\rangle$ slip system continuously resists deformation until a shear strain of 0.60. At a strain of 0.61, the most stretched bond of As1–Ga1 breaks, collapsing the structure and relaxing the shear stress. As a result, the structure becomes layered, which may be considered as a form of "graphitization". The results for bond lengths clearly demonstrate that the As1–Ga1 and As1–Ga2 bonds stretched continuously with an increase in strain. As the shear strain increased from 0.60 to 0.61, the As1–Ga1 bond rapidly increased from 2.53 Å to 2.75 Å, and the As1–Ga2 bond also increased slowly, indicating that the As1–Ga1 bond breaks, while the As1-Ga2 bond remains stable.

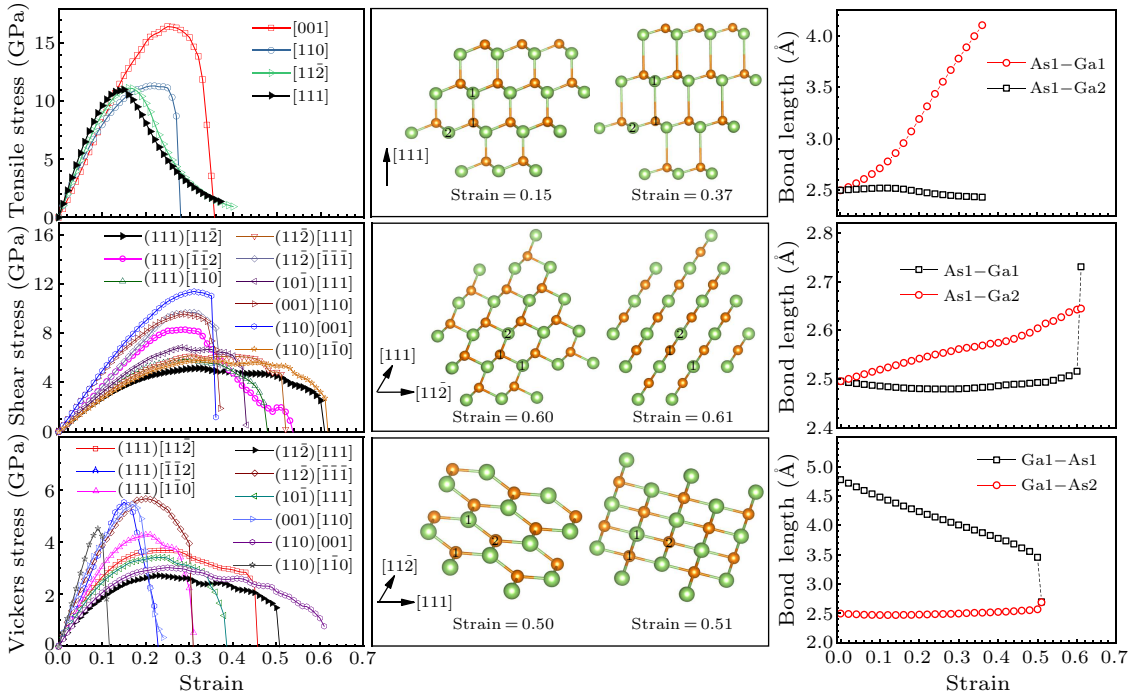

Fig. 1. Structural model and stress and bond-length of flawless GaAs. Left column: Calculated stress-strain curves of single GaAs under tensile, pure shear, and (Vickers) indentation shear deformation. Middle column: structural model evolution under tensile, pure shear, and (Vickers) indentation shear deformation, respectively. Right column: typical bond lengths of GaAs under three types of deformation, with increasing strain (same order).

To investigate the mechanical properties of flawless GaAs, we explored its stress responses under Vickers indentation shear deformation, which imitates the stress conditions occurring in indentation experiments. The weakest Vickers shear direction is (11$\bar{2}$) $\langle 111\rangle$, with an ideal Vickers strength of 2.71 GPa. For this plausible slip system under Vickers deformation, the structural evolution is significantly different from that for pure shear deformation. Owing to the normal indentation compressive pressure, the "As–Ga hexagon" gradually occurs, prior to mechanical failure. With the strain increased to 0.51, an As1–Ga1 bond forms, suggesting that the "Ga–As hexagon" becomes a "Ga–As tetragon". The coordination numbers of As and Ga atoms increased from 4 to 6. Our results confirm the process whereby the distance between Ga1 and As1 atoms decreases until a Ga1–As1 bond is formed. However, the Ga1–As2 bond is less stretched.

Next, a two-part nanotwinned structure of GaAs is established along the most plausible slip (111) plane, as shown in Fig. 2. The upper and lower halves of the structure correspond to the (111) $\langle 11\bar{2}\rangle$ and (111) $\langle \bar{1}\bar{1}2\rangle$ directions of a flawless crystal, respectively, as shown in Figs. 2(a)–2(c). The nanotwinned cell has 24 Ga and 24 As atoms. The stacking sequence of a nanotwinned structure can be described as ABC|C′B′A′..., where | denotes the twin plane. The DFT calculation reveals that the energy of nanotwinned GaAs is −4.132 eV/atom, which is close to that of flawless crystal GaAs (−4.136 eV/atom). Such a small difference in energy may explains the strong tendency to twin in the growth of GaAs compound semiconductors.[56] Taking into account the quantum confinement effect,[57,58] the Vickers hardness of single crystalline nanotwinned GaAs measures up to 19.2 GPa. To explore the strength of the nanotwinned structure, we determined the stress-strain relation of nanotwinned GaAs by means of a comparison with that of the single crystal along its most plausible slip system, (111) $\langle 11\bar{2}\rangle$, as presented in Fig. 3(a). The ideal pure shear strength of nan-

otwinned GaAs is 5.87 GPa at the first maximum shear stress, which is 14% higher than that of the flawless crystal (5.15 GPa).

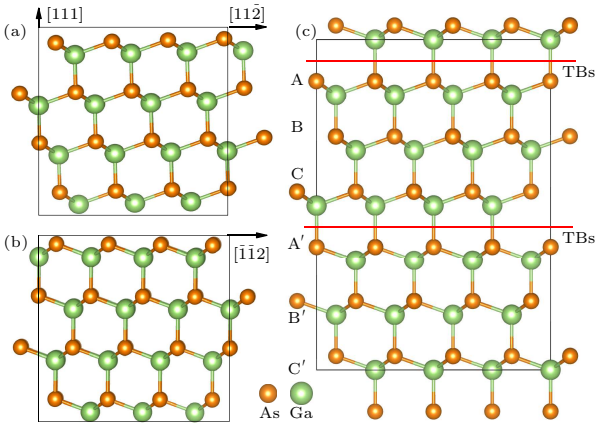

Fig. 2. Atomic structures for crystal and nanotwinned GaAs. (a) Atomic structure for crystalline GaAs based on the (111) ⟨11$\bar{2}$⟩ slip system. (b) Atomic structure for crystalline GaAs based on the (111) ⟨$\bar{1}\bar{1}$2⟩ slip system. (c) Nanotwinned GaAs structure, with the TB along the {111} plane.

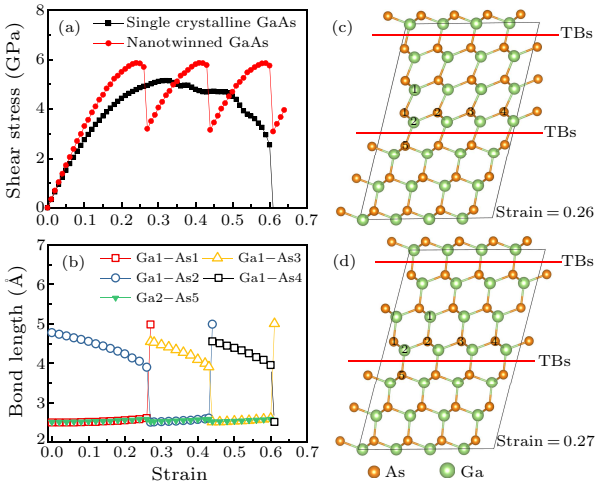

Fig. 3. (a) Stress-strain relations for nanotwinned GaAs, together with a comparison with crystalline GaAs along the most plausible slip system (111) ⟨11$\bar{2}$⟩. (b) Typical bond length (Ga1–As1, Ga1–As2, Ga1–As3, Ga2–As5) with increasing pure shear strain. (c) Nanotwinned structure at 0.26 strain, prior to rearrangement. (d) Nanotwinned structure at 0.27 strain, following rearrangement.

We examined the structural deformation and bond-responding processes to explore the essential strengthening mechanism of nanotwinned GaAs. The results in Figs. 3(b)–3(d) provide structural snapshots and illustrate bond changes in nanotwinned GaAs at critical pure shear strain. The nanotwinned structure continuously resists pure shear deformation, up to a shear strain of 0.26. At a shear strain of 0.27, the stretched As1-Ga1 bond suddenly changes from 2.61 to 5.00 Å, as shown in Fig. 3(b), indicating that the bond breaks. At the same time, the As2–Ga1 distance decreases from 3.89 to 2.50 Å, representing the formation of a new covalent bond. The nanotwinned structure of the upper half moves to the right by one "Ga–As hexagon", due to the bond-breaking and bond-formation process, as indicated in Figs. 3(c)–3(d). This rearranged process releases the pure shear stress, reducing it from 5.70 to 3.20 GPa. Since the stress does not fall below 0 GPa, the nanotwinned structure could potentially further resist deformation with increasing shear strain. As the shear strain increases from 0.43 to 0.44, the same process of bond breaking and formation (the Ga1–As2 bond breaks while the Ga1–As3 bond forms) occurs. The same process also takes place where shear strain increases from 0.60 to 0.61, in that the Ga1–As3 bond breaks, and a Ga1–As4 bond forms. The Ga2–As5 bond at the twin boundary does not continue this rapid increase, and we therefore believe that the layer "hexagon" does not move. We can consider that the nanotwinned structure does not change on the whole, subsequent to the bond breaking-formation process. For the latter two rearranged processes, the maximum shear stress measures 5.86 and 5.85 GPa respectively, which is similar to the first maximum shear stress of 5.87 GPa. These values further confirm that the nanotwinned structure can be regarded as unchanged following the bond breaking-formation process.

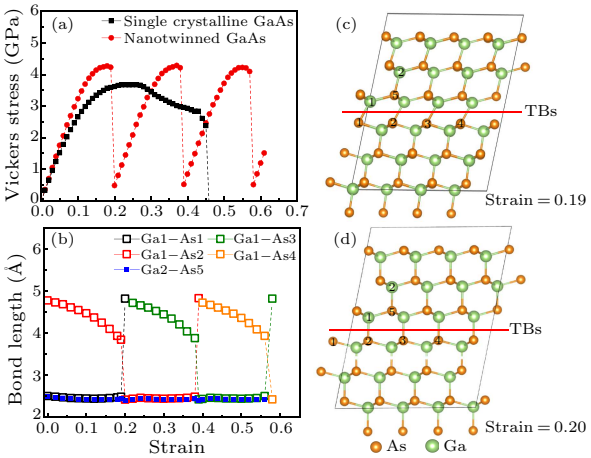

Fig. 4. (a) Stress-strain relations for nanotwinned GaAs under Vickers indentation shear, together with a comparison with crystalline GaAs along (111) ⟨11$\bar{2}$⟩. (b) Typical bond length (As1–Ga2, As3–Ga4) and atomic distance (Ga1–As1, Ga1–As2, Ga1–As3, Ga2–As5) with increasing Vickers indentation shear strain. (c) Nanotwinned structure at 0.19 strain, prior to rearrangement. (d) Nanotwinned structure at 0.20 strain, after rearrangement.

As illustrated in Fig. 4, the stress-strain relation, structural snapshot, and bond change under indentation shear deformation were examined. The first maximum shear stress of the nanotwinned GaAs is 4.27 GPa, which is 16% higher than that of flawless crystal, as shown in Fig. 4(a). As the strain increases from 0.19 to 0.20, the Ga1–As1 bond rapidly increases,

indicating the bond breaking, while a Ga1–As2 bond forms, as presented in Fig. 4(b). Compared to the upper and lower parts of nanotwinned structure, the twin boundary is seriously distorted, as shown in Fig. 4(c). The process moves the top three layers to the right by one "Ga–As hexagon", and the last two bond breaking-formation processes are the same as those for the first changes, as presented in Fig. 4(d). The deformation pattern of nanotwinned GaAs under Vickers shear loading is similar to that of pure shear. The main difference is that the location of the bond is rearranged; the layer of bond rearrangement occurs over the twin boundary for pure shear deformation, but the bond breaking-formation process occurs at the twin boundary under Vickers indentation shear.

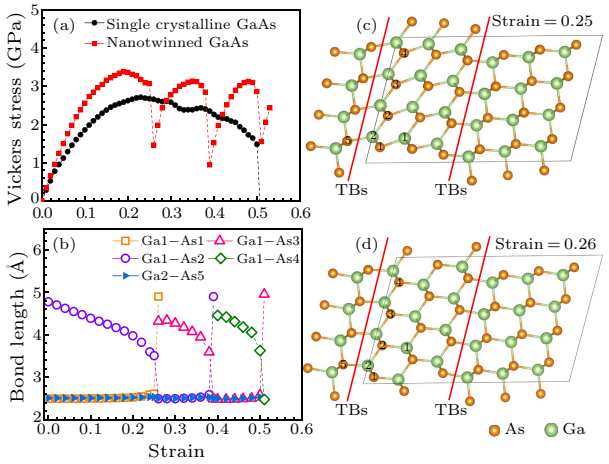

Fig. 5. (a) Stress-strain relations for nanotwinned GaAs under Vickers indentation shear, together with a comparison with crystalline GaAs along $(11\bar{2})$ $\langle 111\rangle$. (b) Typical bond length with the increasing Vickers indentation shear strain. (c) Nanotwinned structure at 0.25 strain, prior to rearrangement. (d) Nanotwinned structure at 0.26 strain, after rearrangement.

For further insights into the strengthening of nanotwinned GaAs, we applied Vickers indentation shear deformation to the nanotwinned structure, and compared it to flawless crystal along the weakest direction of $(11\bar{2})$ $\langle 111\rangle$. The results in Fig. 5(a) show that the maximum shear stresses of the nanotwinned GaAs are 3.37, 3.12, and 3.12 GPa, which are 15% higher than that for a flawless crystal along the $(11\bar{2})$ $\langle 111\rangle$ direction under indentation shear deformation. As the strain increases from 0.25 to 0.26, the Ga1–As1 bond breaks, and a Ga1–As2 bond forms, as shown in Fig. 5(b). Our results show that the left side is more seriously distorted, but that the right side of the nanotwinned structure remains almost unchanged, as shown in Figs. 5(c)–5(d). Thus, the presence of a twin boundary suppresses structural failure, as compared with flawless GaAs under Vickers shear loading.

The above results show that the nanotwinned GaAs displays much greater mechanical strength, as compared with the single crystalline phase. To investigate the influence of nanotwinning on electronic properties, the calculated density of states (DOS) of crystal and nanotwinned GaAs are shown in Fig. 6. The theoretical electronic band gap of the single crystalline phase is 0.16 eV, which agrees well with previous theoretical results.[59–61] For the nanotwinned GaAs structure, the calculated electronic band gap is 0.17 eV, which is almost identical to that for the single phase. Our results show that the theoretical electronic density of states (DOS) is not adversely affected by nanotwinning, a useful insight in terms of the development of reliable electronic devices with superior mechanical properties in the future.

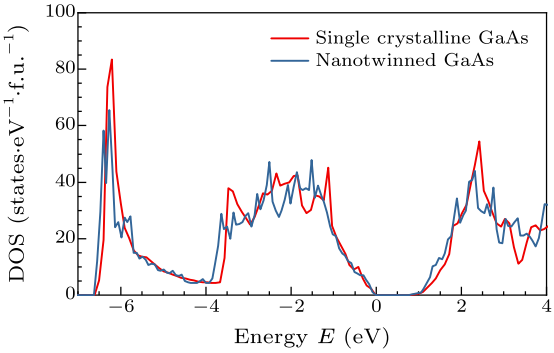

Fig. 6. Calculated electronic density of states (DOS) for single crystalline GaAs and nanotwinned GaAs.

In summary, systematic first-principles calculations have been used in this work to investigate the ideal strength and failure mechanism of GaAs. Our results reveal that the (111) $\langle 11\bar{2}\rangle$ of flawless GaAs is the most plausible slip system under pure shear deformation, with an ideal strength of 5.15 GPa. The $(11\bar{2})$ $\langle 111\rangle$ slip system, with an ideal Vickers strength of 2.71 GPa, is the weakest direction under indentation loading conditions. We have also examined the role of the nanotwinned structure in enhancing the mechanical properties of covalent semiconductor GaAs. The intrinsic mechanical strengths of nanotwinned GaAs are 14% and 15% higher than flawless crystal under pure shear deformation and Vickers shear deformations, respectively. This superior strength originates from a directional covalent bond rearrangement at the twin boundary in nanotwinned GaAs; this represents a possible strategy for enhancing the mechanical properties of semiconductors without producing a significantly negative effect on their electronic performance.

References

[1] Masataka H, Kohei S, Hisashi M, Yoshinao K, Akinori K, Akito K, Takekazu M and Shigenobu Y 2016 *Sci. Technol.* **31** 034001
[2] Jose M, Philippe G, Xavier P, Amador P T and Jose R 2014 *IEEE Trans. Power Electron.* **29** 2155
[3] Rahul K, Mukhopadhyay P, Bag A, Jana S K, Chakraborty A, Das S, Mahata M K and Biswas D 2015 *Appl. Surf. Sci.*

324 304
[4] Zhao X Y, Huang J H, Zhuo Z Y, Xue Y Z, Ding K, Dou X M, Liu J and Sun B Q 2020 *Chin. Phys. Lett.* **37** 044204
[5] Gao L, Liu Q L, Yang J W, Wu Y, Liu Z H, Qin S J, Ye X B, Jin S F, Li G D, Zhao H Z and Long Y W 2020 *Chin. Phys. Lett.* **37** 066202
[6] Zhou J J and Marco B 2016 *Phys. Rev. B* **94** 201201
[7] Zhang B W, Nie Z G, Wang B, Wang D K, Tang J L, Wang X H, Zhang J H, Xing G H, Zhang W C and Wei Z P 2020 *Phys. Chem. Chem. Phys.* **22** 25819
[8] Zhang S H, Xu W, Badalyan S M and Peeters F M 2013 *Phys. Rev. B* **87** 075443
[9] Takayuki S, Ryuichi M and Tohru O 2013 *Phys. Rev. Lett.* **111** 057005
[10] Frank D, Matthias G, Paul B, Ulrich F, Christian K, Thomas N D T, Eduard O, Gerald S, Michael S, Alexander W, AndreasW B, Rainer K, Matteo P, Nicolas B, Charlotte D, Eric G, Bruno G, Thierry S, Aurélie T, Thomas S, Anja D, Thomas H and Klaus S 2014 *Prog. Photovoltaics* **22** 277
[11] Josef A C, David A T and Ray R L 2009 *Nano Lett.* **9** 148
[12] Jongseung Y, Sungjin J, Chun I S, Inhwa J, Hoon-Sik K, Matthew M, Etienne M, Li X L, James J C, Ungyu P and John A R 2010 *Nature* **465** 329
[13] Sandroff C J, Hegde M S, Farrow L A, Bhat R J P and Chang C C 1990 *J. Appl. Phys.* **67** 586
[14] Muhammad U, Christopher A B, Andrew L and Eoin P O R 2011 *Phys. Rev. B* **84** 245202
[15] Grillo S E, Ducarroir M, Nadal M, Tournie E and Faurie J P 2003 *J. Phys. D* **36** L5
[16] Lee J, Wu J, Shi M X, Jongseung Y, Sang-Il P, Li M, Liu Z J, Huang Y G and Rogers J A 2011 *Adv. Mater.* **23** 986
[17] Laister D and Jenkins G M 1973 *J. Mater. Sci.* **8** 1218
[18] Wang J K, Li S S, Wang N, Liu H J, Su T C, Hu M H, Han F, Yu K P and Ma H A 2019 *Chin. Phys. Lett.* **36** 046101
[19] Lu K, Lu L and Suresh S 2009 *Science* **324** 349
[20] Wang Z C, Mitsuhiro S, Keith P M, Gu L, Susumu T, Alexander L S and Yuichi I 2011 *Nature* **479** 380
[21] Gao B, Gao P Y, Lu S H, Lv J, Wang Y C and Ma Y 2019 *Sci. Bull.* **64** 301
[22] Lu L, Shen Y F, Chen X H, Qian L H and Lu K 2004 *Science* **304** 422
[23] Madhav R K, Guo J J, Shinoda Y, Fujita T, Hirata A, Singh J P, McCauley J W and Chen M W 2012 *Nat. Commun.* **3** 1052
[24] An Q, Goddard W A, Xie K Y, Sim G D, Hemker K J, Munhollon T, Toksoy M F and Haber R A 2016 *Nano Lett.* **16** 7573
[25] Tian Y J, Xu B, Yu D L, Ma Y M, Wang Y B, Jiang Y B, Hu W T, Tang C C, Gao Y F, Luo K, Zhao Z S, Wang L M, Wen B, He J L and Liu Z Y 2013 *Nature* **493** 385
[26] Liu X Y, Zhang H and Cheng X L 2018 *Chin. Phys. Lett.* **35** 116201
[27] Lu L, Chen X, Huang X and Lu K 2009 *Science* **323** 607
[28] Huang Q, Yu D L, Xu B, Hu W T, Ma Y M, Wang Y B, Zhao Z S, Wen B, He J L, Liu Z Y and Tian Y J 2014 *Nature* **510** 250
[29] Li B, Sun H and Chen C 2014 *Nat. Commun.* **5** 4965
[30] Li G D, Sergey I M, Zhang Q J, An Q, Zhai P C and G J S 2017 *Phys. Rev. Lett.* **119** 215503
[31] Kresse G and Furthmiiller J 1996 *Comput. Mater. Sci.* **6** 15
[32] Kresse G and Joubert D 1999 *Phys. Rev. B* **59** 1758
[33] John P P, Kieron B and Matthias E 1996 *Phys. Rev. Lett.* **77** 3865
[34] Kresse G and Furthmuller J 1996 *Phys. Rev. B* **54** 11169
[35] Zhang Y, Sun H and Chen C 2004 *Phys. Rev. Lett.* **93** 195504
[36] Pan Z, Sun H and Chen C 2009 *Phys. Rev. B* **79** 104102
[37] Pan Z, Sun H, Zhang Y and Chen C 2009 *Phys. Rev. Lett.* **102** 055503
[38] Pan Z, Sun H and Chen C 2007 *Phys. Rev. Lett.* **98** 135505
[39] Qu N R, Wang H C, Li Q, Li Z P and Gao F M 2019 *Chin. Phys. Lett.* **36** 036201
[40] Liu C, Zhai H, Sun Y, Gong W, Yan Y, Li Q and Zheng W 2018 *Phys. Chem. Chem. Phys.* **20** 5952
[41] Li H, Hao Y, Sun D, Zhou D, Liu G, Wang H and Li Q 2019 *Phys. Chem. Chem. Phys.* **21** 25859
[42] Gong W, Liu C, Song X, Li Q, Ma Y and Chen C 2019 *Phys. Rev. B* **100** 220102(R)
[43] Liu C, Song X, Li Q, Ma Y and Chen C 2019 *Phys. Rev. Lett.* **123** 195504
[44] Li Q, Zhou D, Zheng W, Ma Y and Chen C 2015 *Phys. Rev. Lett.* **115** 185502
[45] Liu C, Song X, Li Q, Ma Y and Chen C 2020 *Phys. Rev. Lett.* **124** 147001
[46] Lu C, Gong W, Li Q and Chen C 2020 *J. Phys. Chem. Lett.* **11** 9165
[47] Blakemore J S 1982 *J. Appl. Phys.* **53** R123
[48] Wu Z J, Zhao E J, Xiang H P, Hao X F, Liu X J and Meng J 2007 *Phys. Rev. B* **76** 054115
[49] Hill R 1952 *Proc. Phys. Soc. London Sect. A* **65** 349
[50] Vurgaftman I, Meyer J R and Ram-Mohan L R 2001 *J. Appl. Phys.* **89** 5815
[51] Chen X Q, Niu H Y, Li D Z and Li Y Y 2011 *Intermetallics* **19** 1275
[52] Gao F M, He J L, Wu E D, Liu S M, Yu D L, Li D C, Zhang S Y and Tian Y J 2003 *Phys. Rev. Lett.* **91** 015502
[53] Zhang M, Liu H, Li Q, Gao B, Wang Y, Li H, Chen C and Ma Y 2015 *Phys. Rev. Lett.* **114** 015502
[54] Li B, Sun H and Chen C 2016 *Phys. Rev. Lett.* **117** 116103
[55] Gong W, Wang M, Liu C, Qin Z, Liu Y, Zhang X, Li Q and Zheng W 2017 *J. Phys. Chem. C* **121** 26457
[56] Chen T P, Chen F R, Chuang Y C, Guo Y D, Peng J G, Huang T S and Chen L J 1992 *J. Cryst. Growth* **118** 109
[57] Tse J S, Klug D D and Gao F M 2006 *Phys. Rev. B* **73** 140102R
[58] Zhao Z S, Xu B and Tian Y J 2016 *Annu. Rev. Mater. Res.* **46** 383
[59] Tahini H A, Chroneos A, Murphy S T, Schwingenschlögl U and Grimes R W 2013 *J. Appl. Phys.* **114** 063517
[60] Philip P R, Stewart J C and David J T 2001 *Phys. Rev. B* **63** 115206
[61] Rashid A, S J H, Hadi A, Maqsood A and Fazal A 2007 *Comput. Mater. Sci.* **39** 580